Electronic and local atomic structures of $(La_{1-x}Pr_x)_{0.85}Zr_{0.15}MnO_3$ studied by x-ray absorption spectroscopy

2005 J. Phys.: Condens. Matter 17 4197

(http://iopscience.iop.org/0953-8984/17/26/017)

INSTITUTE OF PHYSICS PUBLISHING JOURNAL OF PHYSICS: CONDENSED MATTER

J. Phys.: Condens. Matter **17** (2005) 4197–4205 doi:10.1088/0953-8984/17/26/017

Electronic and local atomic structures of $(La_{1-x}Pr_x)_{0.85}Zr_{0.15}MnO_3$ studied by x-ray absorption spectroscopy

K P Krishna Kumar[1], J W Chiou[1], H M Tsai[1], C W Pao[1], J C Jan[1], P C Hsu[1], D C Ling[1], F Z Chien[1], W F Pong[1,4], M-H Tsai[2] and J F Lee[3]

[1] Department of Physics, Tamkang University, Tamsui, Taiwan 251, Republic of China
[2] Department of Physics, National Sun Yat-Sen University, Kaohsiung, Taiwan 804, Republic of China
[3] National Synchrotron Radiation Research Center, Hsinchu, Taiwan 300, Republic of China

E-mail: wfpong@mail.tku.edu.tw

Received 21 March 2005, in final form 18 May 2005
Published 17 June 2005
Online at stacks.iop.org/JPhysCM/17/4197

Abstract

Mn $L_{3,2}$-, K-, O K- and Pr $M_{5,4}$-edge x-ray absorption near-edge structure (XANES) spectra of $(La_{1-x}Pr_x)_{0.85}Zr_{0.15}MnO_3$ (LPZMO) with $x = 0$, 0.05, 0.1, 0.15 and 0.2 were measured to study the electronic structure and the effect of Pr substitution. An analysis of Mn $L_{3,2}$- and K-edge spectra indicates that LPZMO is an electron-doped system. Pr substitution is found to increase the average effective charge of Mn ions and to induce an additional unoccupied majority spin (↑ spin) e_g subband in the Mn $L_{3,2}$-edge XANES spectrum. Mn $L_{3,2}$-, O K- and Pr $M_{5,4}$-edge XANES results demonstrate that the substitution of La ions by smaller Pr ions changes O 2p–Mn 3d and O 2p–Pr 4f hybridized states. Extended x-ray absorption fine structure (EXAFS) analysis at the Mn K edge reveals clear changes in local atomic structure around Mn ions due to the Pr substitution. XANES and EXAFS analyses show a small distortion in the MnO_6 octahedron or a disorder in the lattice, which may be due to localization of charge carriers and/or the increased effective positive charge of Mn ions.

1. Introduction

Hole-doped lanthanum manganites of the form $RAMnO_3$ (R = rare earth and A = divalent cation) have been investigated extensively owing to their potential technological applications. They exhibit properties such as colossal magnetoresistance (CMR), charge, spin and orbital ordering transitions and anomalous magnetization [1–5]. Despite these extensive studies, the fundamental origins of these properties still remain controversial. Millis *et al* [6] proposed

[4] Author to whom any correspondence should be addressed.

a polaronic model of dynamic Jahn–Teller (JT) distortion of the MnO_6 octahedron beyond the double-exchange mechanism that involves O-ion-mediated exchange of Mn^{3+} and Mn^{4+} ions. Das and Mandal reported CMR behaviour in the electron-doped $La_{1-x}Ce_xMnO_3$ and suggested that CMR probably occurs in a system of a mixed-valence state of Mn^{2+}–Mn^{3+} [7]. A study by Asokan *et al* on the electronic structure of $La_{0.7}Ce_{0.3}MnO_3$ indicated that Ce dopants increase the occupation of Mn 4p as well as majority spin e_g orbitals, which reduces the positive effective charge of Mn ions [8]. They also found that holes are induced in O 2p-derived states due to Ce doping. The main disadvantage of the Ce-doped sample is that Mn ions in the sample may have various oxidation states due to possible existence of Ce^{3+} and Ce^{4+} mixed valence states. Therefore, it is of considerable research interest to investigate if the CMR effect exists in compounds in which La^{3+} is partially substituted by another tetravalent element [9–11]. More recently, it was found that $(La_{1-x}Pr_x)_{0.85}Zr_{0.15}MnO_3$ (LPZMO) exhibits CMR behaviour [12]. The advantage of Zr over Ce doping is that the Zr-doped single-phase sample can be easily prepared and has a Zr^{4+} single-valence state. The magnetoresistance (MR) ratio of LPZMO and the metal–insulator transition temperature (T_{MI}) were observed to increase and decrease, respectively, with the increase of the Pr content [12]. It has been suggested that the reduction of the average A-site ionic radius by partial substitution of La ions by smaller ions could result in structural distortion around the La ion, which may play an important role in magnetic as well as electrical properties of manganites [3, 13]. The knowledge of the valence of Mn ions and interactions between constituent ions in LPZMO may elucidate the origins of the observed magneto-transport properties. Since x-ray absorption spectroscopy is well established as a suitable tool for investigating the electronic structure and local atomic environment, x-ray absorption near-edge structure (XANES) measurements at the Mn $L_{3,2}$, K, O K and Pr $M_{5,4}$ edges were performed to investigate the effect of Pr substitution on the electronic and atomic structures of LPZMO.

2. Experiment

XANES spectra were obtained using the facility at the National Synchrotron Radiation Research Center, Hsinchu, Taiwan, operating at electron energy of 1.5 GeV and a maximum stored current of 200 mA. O K, Pr $M_{5,4}$ and Mn $L_{3,2}$ edges were measured using the high-energy spherical grating monochromator (HSGM) beamline in the fluorescence and sample current modes, respectively, while the Mn K-edge extended x-ray absorption fine structure (EXAFS) was measured using the wiggler-C beamline with the Si(111) double-crystal monochromator in the transmission mode. The typical resolution of the HSGM beam line was 0.2 eV and that of the wiggler-C beamline was 0.6 eV. The LPZMO samples were synthesized by the standard solid-state reaction method. Stoichiometric powders of La_2O_3, ZrO_2, Mn_2O_3 and Pr_6O_{11} were calcined in air at 950–1000 °C for 12 h three times. They were then sintered in air at 1250 °C for 24 h. The cooling rate in each case was 2 °C min^{-1}. Powdered LPZMO samples with $x = 0$, 0.05, 0.1, 0.15 and 0.2 were chosen in the present study and the reference materials were MnO, Mn_2O_3, MnO_2 and Pr_6O_{11}. Room-temperature x-ray diffraction measurements of LPZMO for various values of x are shown in figure 1. All samples are single-phase compounds with a rhombohedral lattice of space group $R\bar{3}C$. Details of the preparation and characterization are presented elsewhere [12].

3. Results and discussion

Figure 2 presents the normalized Mn $L_{3,2}$-edge XANES spectra of LPZMO and references MnO, Mn_2O_3 and MnO_2. After pre-edge background subtraction, the spectra were normalized

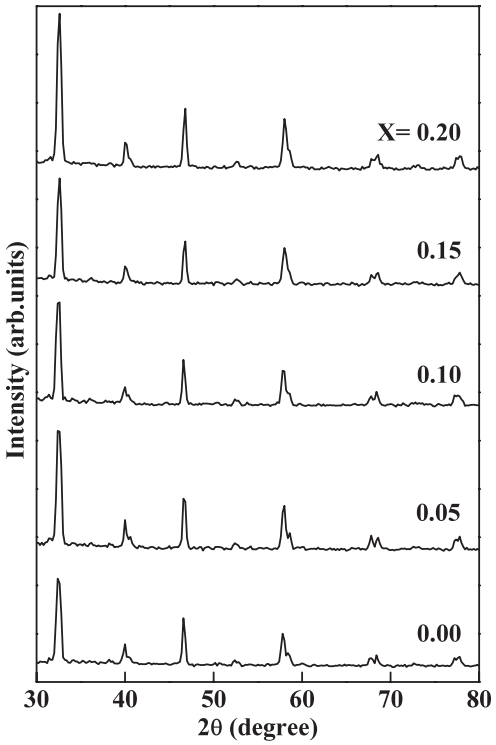

Figure 1. X-ray diffraction measurements of LPZMO for various values of x.

to the same area in the energy range between 665 and 670 eV (not fully shown). Generally, XANES spectra are sensitive to the crystal field symmetry. The spin–orbit interaction of the Mn 2p core states splits the spectrum into two broad multiplets, namely the L_3 ($2p_{3/2}$) edge around 644 eV and the L_2 ($2p_{1/2}$) edge around 655 eV. Each of these two regions is further split into t_{2g}- and e_g-orbital features because of the crystal-field effect of neighbouring ions. These spectra show valence-specific multiplet structure with a chemical shift due to the change in the oxidation state [14, 15]. Mn ions have 2+, 3+, and 4+ valence states in the MnO, Mn_2O_3 and MnO_2 reference binary oxides, respectively. A close inspection of figure 2 illustrates that the peak position of the double-peak spectral feature of LPZMO at the L_3 edge is close to those of Mn_2O_3 and MnO, suggesting that the average oxidation state of the Mn ion is between 2+ and 3+. In the Mn^{2+} state, the three t_{2g} and two e_g orbitals are each filled with one majority spin (↑ spin) electron. The unoccupied minority spin (↓ spin) t_{2g} and e_g subbands contribute to features A_1 and B_1. In the Mn^{3+} state, the Mn ion loses one ↑ spin e_g electron, so that the ↑ spin e_g subband also contributes to the Mn $L_{3,2}$-edge spectrum. The intensity of feature B_1 is increased in the Pr-substituted samples. Thus, the Pr substitution increases the average effective positive charge on the Mn ion, which can potentially create polaronic distortions in LPZMO. Alternatively, it could cause a JT distortion around the Mn site, since Mn^{3+} is a JT ion. The distortion was observed to increase the MR ratio from 45% to 70% near T_{MI} as x varies from 0 to 0.20 in a field of 7 T [12]. Furthermore, broadening and splitting and/or appearance of new peaks are also observed at the L_3 edge with Pr substitution. These changes in the spectrum are attributable to changes in the symmetry of the 3d states of Mn ions due to the crystal-field effect of neighbours.

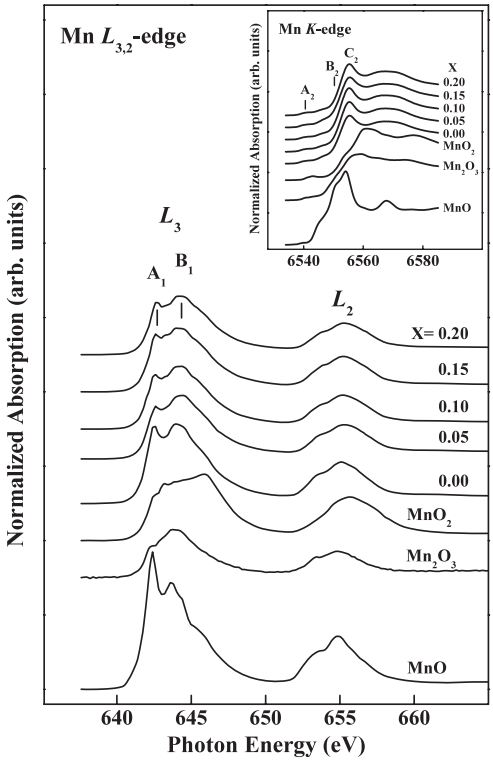

Figure 2. Normalized Mn $L_{3,2}$-edge XANES spectra of LPZMO for various values of x and reference samples. The inset presents normalized Mn K-edge XANES spectra of LPZMO for various values of x and reference samples.

The inset in figure 2 presents the normalized Mn K-edge XANES spectra of LPZMO and references. These spectra are dominated by the Mn 1s to 4p dipole transition. The very weak pre-edge feature A_2 was attributed to the quadrupole transition from 1s to Mn 3d states by Yamaguchi *et al* [16] and by Subias *et al* [17]. Subias *et al* argued that this relatively broad feature results from transition of the Mn 1s electron into empty Mn 3d–O 2p hybridized states under the influence of an octahedral ligand field. They also argued that the mixed valence states of Mn might lead to a mixture of 1s to 3d transition energies, which broaden this pre-edge feature. Feature B_2 reveals the p character of the lowest Mn 3d-like electronic band due to hybridization. Feature C_2 in the LPZMO spectra resembles more closly those of Mn_2O_3 and MnO than that of MnO_2, which suggests that the average oxidation state of Mn ions is between 2+ and 3+ and is in consistence with Mn $L_{3,2}$-edge XANES results.

Figure 3 displays O K-edge XANES spectra of LPZMO and references MnO, Mn_2O_3, MnO_2 and Pr_6O_{11}, which probe the local density of unoccupied O 2p states above the Fermi level. After pre-edge background subtraction, the spectra were normalized using incident beam intensity I_0 and by keeping the same area in the energy range between 555 and 565 eV (not fully shown). Features A_3, B_3 and C_3 are associated with O 2p–Mn 3d, O 2p–La 5d/Pr 5d/Zr 4d and O 2p–Mn 4sp hybridized states, respectively [18–20]. As shown in figure 3, the spectra of LPZMO differ drastically from those of reference samples. Feature A_3 in the spectra of LPZMO (∼532.8 eV) was attributed to the multiplet structure of Mn 3d states with t_{2g} and e_g symmetry due to the crystal-field effect and coulomb interaction [21]. Feature A_3 in

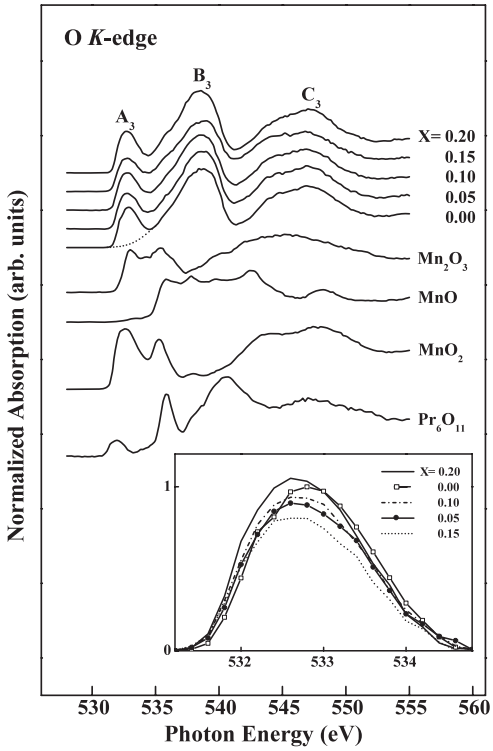

Figure 3. Normalized O K-edge XANES spectra of LPZMO for various values of x and reference samples. The inset magnifies peak A_3 after background subtraction.

the spectra of Pr_6O_{11} (∼532 eV) is associated with O 2p–Pr 4f hybridized states. Therefore, the contributions of Pr 4f and Mn 3d bands may overlap in the spectra of LPZMO. The inset shows a magnified view of feature A_3 after background subtraction using a best-fitted Gaussian curve as indicated by the dotted lines. The intensities of feature A_3 for $x = 0$ to 0.20 do not show a clear trend, which might be due to a disorder in the lattice during the initial stages of Pr substitution. It is well established that both valence and conduction bands in CMR materials contain Mn 3d and O 2p hybridized states [22]. Any variation in O 2p–Mn 3d hybridization is believed to affect electronic states near the Fermi level. The additional features at the lower energy side of feature B_3 may originate from O 2p–Pr 5d/Zr 4d hybridized orbitals [23]. The minor changes in feature C_3 as the Pr content increases can be attributed to the slight distortion of the local structure caused by the substitution of La ions with a covalent radius of 1.160 Å by smaller Pr ions with a covalent radius of 1.126 Å for Pr^{3+} and 0.960 Å for Pr^{4+} [23].

Figure 4 presents the Pr $M_{5,4}$-edge XANES spectra of LPZMO and the reference Pr_6O_{11}. After pre-edge background subtraction, the spectra were normalized with the area in the energy range between 964 and 969 eV kept fixed. The figure measures the number of unoccupied Pr 4f states above the Fermi level. These spectra are highly sensitive to the valence state and the distribution of valence electrons between metal and ligand orbitals. These experimental structures can be well reproduced by atomic multiplet calculations [24, 25]. The major peaks in the spectra, A_4 and B_4, are attributable to electronic transitions from Pr $3d_{5/2}$ and $3d_{3/2}$ states, respectively, to 4f states, and the separation between peaks A_4 and B_4 is due to Pr 3d spin–orbit interaction. The 4f electrons are highly localized and interact weakly with the

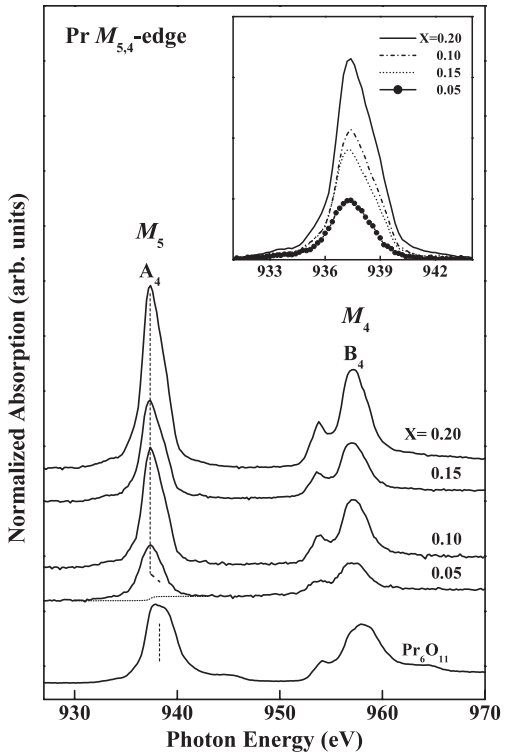

Figure 4. Normalized Pr $M_{5,4}$-edge XANES spectra of LPZMO for various values of x and a reference sample. The inset magnifies peak A_4.

environment. They determine the magnetic property of the material, but are not involved in the chemical bonding. $M_{5,4}$-edge spectra of trivalent rare earth elements are shifted to lower energy by more than 1 eV with a decrease in their valence [26]. The valence of Pr in Pr_6O_{11} is about 3.67. The lower energy shift (∼0.5 eV) of the LPZMO A_4 peak (indicated by the vertical line) suggests that the Pr valence in LPZMO is less than 3.67. The inset magnifies the A_4 peak after background subtraction using a best-fitted arctangent function as shown by the dotted lines. The variation in the peak intensity correlates with the change of the Pr 4f occupancy and hybridization of 4f orbitals with conduction-electron states. The inset shows an increase in the peak intensity by Pr substitution, which suggests an increase in the number of Pr 4f unoccupied states and an increase of charge loss in occupied Pr 4f states as x is increased. However, there is an exception for $x = 0.15$, which may be due to a disorder in the lattice caused by Pr substitution or due to localization of charges. This phenomenon is similar to that of high-temperature superconducting cuprates [22, 27].

Figure 5 displays the Fourier transform (FT) of the EXAFS $k^3\chi$ data at the Mn K edge, which describes the local atomic structure around the Mn atoms. The inset presents Mn K-edge $k^3\chi$ data of the EXAFS oscillations. It is well known that the crystal structure of the ABO_3 type of perovskite-like $LaMnO_3$ undergoes two main types of distortion. One is the local tetragonal JT distortion of oxygen atoms around each Mn site and the other is the tilt of the MnO_6 octahedron. Due to the reduced symmetry by distortion, the EXAFS $k^3\chi$ data shown in the inset of figure 5 look noisy. To quantitatively obtain all bond lengths and Debye–Waller factors requires the analysis using the UWXAFS code, which involves a combination

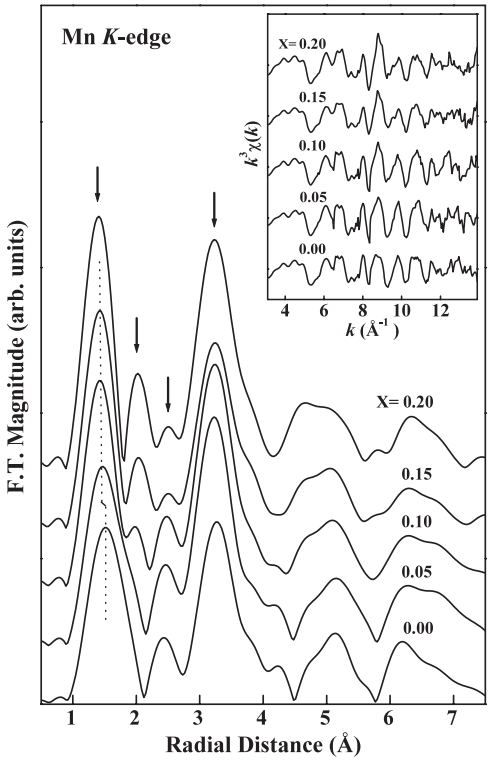

Figure 5. Magnitude of Fourier transform of the EXAFS $k^3\chi$ data at the Mn K edge from $k = 3.5$ to 12.5 Å for various values of x. The inset displays $k^3\chi$ data of the Mn K-edge EXAFS oscillations.

of multiple-scattering EXAFS computer program FEFF and nonlinear least-squares-fitting computer program FEFFIT. There are 16 parameters to fit to the EXAFS data at each x value up to the first four shells. However, the properties of the first few shell peaks in the FT spectrum, which contain information of the nearest-neighbour (NN) Mn–O bond and distances between Mn and neighbouring cations, suffice for the purpose of finding the local bonding structure of Mn.

The position of the first shell peak, ∼1.51 Å (indicated by the first vertical arrow), reflects the NN Mn–O bond length. The increase in the amplitude and the decrease in FWHM (full width at half maximum) of this peak indicate a reduction in the local atomic distortion of the MnO_6 octahedron or a less distorted oxygen environment around Mn atoms. A similar effect was observed in Ca-doped $LaMnO_3$ [28]. The position and FWHM of this peak as functions of x are tabulated in table 1. The position of this peak (defined at the maximum) shifts slightly towards a lower radial distance as x increases from 0 to 0.10 (as indicated by the vertical dotted line) and remains approximately unchanged for $x > 0.1$. This finding suggests that Pr substitution slightly reduces the NN Mn–O bond length, which may be related to a slight increase in the Mn effective charge and a reduction of the Debye–Waller factor with an increase in the Pr content. The second and third peaks (indicated by the second and third vertical arrows) were attributed to the next-nearest-neighbour Mn–Pr/Zr and Mn–La distances, respectively [28, 29]. The intensities of the second and third peaks increase and decrease, respectively, as the Pr content increases, which may simply reflect the increase (decrease) of the Pr (La) content when more La ions are substituted by Pr ions. The peak at

Table 1. The first shell peak position and the corresponding FWHM as a function of x.

x	Peak position	FWHM
0.00	1.51	0.68
0.05	1.47	0.68
0.10	1.41	0.49
0.15	1.41	0.48
0.20	1.41	0.46

$\sim$3.2 Å (indicated by the fourth vertical arrow) corresponds to the Mn–Mn distance, which is essentially independent of the Pr content and suggests that the Pr substitution does not significantly affect the Mn sub-lattice or the arrangement of the MnO_6 octahedra.

The tilt of the MnO_6 octahedron depends on the tolerance factor, $t = (d_{A-O})/\sqrt{2}(d_{B-O})$, which is a geometrical parameter describing mismatch between the sizes of A- and B-site ions in the compound. When the d_{A-O}/d_{B-O} size ratio is exactly $\sqrt{2}$, $t = 1$, and there is no mismatch. When $t < 1$, the octahedron tilts and rotates to reduce the excess space around the A-site rather than a simple shortening of bond distances. This is the case for LPZMO, since $d_{B-O} = d_{Mn-O} \sim 1.97$ Å and d_{A-O} = average of d_{La-O}, d_{Pr-O} and $d_{Zr-O} \sim 2.38$ Å. (Note that the covalent radii of La, Pr, Zr, Mn and O are 1.69, 1.65, 1.45, 1.17 and 0.75 Å, respectively [30].) The d_{A-O}/d_{B-O} size ratio argument is supported by the Mn K-edge EXAFS measurements, which indicate that the NN Mn–O bond length decreases only slightly with an increase in the Pr content. As for the tilt and rotation of the MnO_6 octahedron, Hsu and Ling found that there is a change in the Mn–O–Mn bond angle as revealed from the Rietveld refinement result of XRD data [12]. Hsu and Ling argue that the variation in the ionic radii of La and Pr of $\sim$3% may introduce a microstructural inhomogeneity in LPZMO.

4. Conclusion

The Mn $L_{3,2}$ and K-edge XANES results indicate that LPZMO with the partial substitution of La by Zr is an electron-doped system. Pr substitution is found to increase the average effective positive charge on the Mn ions. The Mn L_3-edge analysis reveals that the Mn $L_{3,2}$-edge XANES spectra contain an additional unoccupied $\uparrow$ spin e_g subband resulting from Pr substitution. The Mn $L_{3,2}$-, O K- and Pr $M_{5,4}$-edge XANES results demonstrate changes in the O 2p–Mn 3d and O 2p–Pr 4f hybridization due to the substitution of La by smaller Pr. The EXAFS analysis clearly shows changes in local atomic structure around the Mn atoms caused by Pr substitution. XANES and EXAFS analyses reveal a reduced distortion in the MnO_6 octahedron or a local disorder in the lattice, which may be caused by the localization of charge carriers and/or an increase in the average effective positive charge on the Mn ions.

Acknowledgments

The authors (KPK, DCL and WFP) would like to thank the National Science Council (NSC) of the Republic of China for financially supporting this research under contract No NSC 93-2112-M-032-018 and NSC 92-2112-M-032-002.

References

[1] Ramirez A P, Schiffer P, Cheong S-W, Chen C H, Bao W, Palstra T T M, Gammel P L, Bishop D J and Zegarski B 1996 *Phys. Rev. Lett.* **76** 3188

[2] Schiffer P, Ramirez A P, Bao W and Cheong S W 1995 *Phys. Rev. Lett.* **75** 3336

[3] Millis A J 1998 *Nature* **392** 147
[4] Jin S, Tiefel T H, McCormack M, Fastnacht R A, Ramesh R and Chen L H 1994 *Science* **264** 413
[5] Coey J M D, Viret M and von Molnar S 1999 *Adv. Phys.* **48** 167
[6] Millis A J, Litlewood P B and Shraiman B I 1995 *Phys. Rev. Lett.* **74** 5144
Millis A J, Shraiman B I and Mueller R 1996 *Phys. Rev. Lett.* **77** 175
[7] Das S and Mandal P 1997 *Phys. Rev.* B **56** 15073
[8] Asokan K, Jan J C, Rao K V R, Chiou J W, Tsai H M, Mookerjee S, Pong W F, Tsai M-H, Kumar R, Husain S and Srivastava J P 2004 *J. Phys.: Condens. Matter* **16** 3791
[9] Guo X, Chen Z, Dai S, Zhou Y, Li R, Zhang H, Shen B and Cheng H 2000 *J. Appl. Phys.* **88** 4758
[10] Tan G T, Dai S, Duan P, Zhou Y L, Lu H B and Chen Z H 2003 *Phys. Rev.* B **68** 014426
[11] Tan G, Duan P, Yang G, Dai S, Cheng B, Zhou Y L, Lu H B and Chen Z H 2004 *J. Phys.: Condens. Matter* **16** 1447
[12] Hsu P C and Ling D C 2005 unpublished
[13] Whangbo M H and Torardi C C 1990 *Science* **249** 1143
[14] Liu R S, Jang L Y, Chen J M, Wu J B, Liu R G, Lin J G and Huang C Y 1998 *Solid State Commun.* **105** 605
[15] Kawai J, Mizutani Y, Sugimura T, Sai M, Higuchi T, Harada Y, Ishiwata Y, Fukushima A, Fujisawa M, Watanabe M, Maeda K, Shin S and Gohshi Y 2000 *Spectrochim. Acta* B **55** 1385
[16] Yamaguchi H, Yamada A and Uwe H 1998 *Phys. Rev.* B **58** 8
[17] Subias G, Garcia J, Proietti M G and Blasco J 1997 *Phys. Rev.* B **56** 8183
[18] de Groot F M F, Grioni M, Fuggle J C, Ghijsen J, Sawatzky G A and Petersen H 1989 *Phys. Rev.* B **40** 5715
[19] Abbate M, de Groot F M F, Fuggle J C, Fujimori A, Strebel O, Lopez F, Domke M, Kaindl G, Sawatzky G A, Takano M, Takeda Y, Eisaki H and Uchida S 1992 *Phys. Rev.* B **46** 4511
[20] Abbate M, Cruz D Z N, Zampieri G, Briatico J, Causa M T, Tovar M, Caneiro A, Alascio B and Morikawa E 1997 *Solid State Commun.* **103** 9
[21] Pellegrin E, Tjeng L H, de Groot F M F, Hesper R, Sawatzky G A, Moritomo Y and Tokura Y 1997 *J. Electron Spectrosc. Relat. Phenom.* **86** 115
[22] Ignatov A Yu, Ali N and Khalid S 2001 *Phys. Rev.* B **64** 014413
[23] Murugesan M, Ishigaki T, Kawano H, Chen M, Liu R S and Nachimuthu P 1999 *J. Appl. Phys.* **86** 6985
[24] de Groot F M F 1994 *J. Electron Spectrosc. Relat. Phenom.* **67** 529
[25] de Groot F and van der Laan G 1997 *J. Electron Spectrosc. Relat. Phenom.* **86** 25
[26] Hu Z, Kaindl G and Muller B G 1997 *J. Alloys Compounds* **246** 177
[27] Fehrenbacher R and Rice T M 1993 *Phys. Rev. Lett.* **70** 3471
Liechtenstein A I and Mazin I I 1995 *Phys. Rev. Lett.* **74** 1000
[28] Booth C H, Bridges F, Kwei G H, Lawrence J M, Cornelius A L and Neumeier J J 1998 *Phys. Rev.* B **57** 10440
[29] Subias G, Garcia J, Blasco J and Proietti M G 1998 *Phys. Rev.* B **57** 748
[30] *Table of Periodic Properties of the Elements* 1980 (Skokie, IL: Sargent-Welch Scientific Company)